**Supporting Information**

# Lanthanide Contraction Effect on the Alkaline

# Hydrogen Evolution and Oxidation Reactions

# Activity in Platinum-Rare Earth Nanoalloys

*Carlos A. Campos-Roldán†\*, Raphaël Chattot†, Frédéric. Pailloux‡, Andrea Zitolo,¶
Jacques Rozière†,  Deborah J. Jones†, Sara Cavaliere †\**

† ICGM, University Montpellier, CNRS, ENSCM, 34095 Montpellier cedex 5, France

‡ Institut P', CNRS - Université de Poitiers – ISAE-ENSMA - UPR 3346, 11 Boulevard

Marie et Pierre Curie, Site du Futuroscope, TSA 41123, 86073 Poitiers cédex 9, France

¶ Synchrotron SOLEIL, L'Orme des Merisiers, BP 48 Saint Aubin, 91192 Gif-sur-Yvette,

France


*Corresponding authors:
carlos-augusto.campos-roldan@umontpellier.fr
Sara.Cavaliere@umontpellier.fr


\* Authors to whom correspondence should be addressed.

E-mail:
carlos-augusto.campos-roldan@umontpellier.fr,
Sara.Cavaliere@umontpellier.fr

## S1. Experimental section

*Synthesis of carbon supported Pt-REM nanoalloys*.

0.45 g of carbon Vulcan XC-72 (Cabot), 2 g of $NH_2CN$ (99 %, Sigma-Aldrich), 0.5 g of $H_2PtCl_6 \cdot 6H_2O$ (Sigma-Aldrich) and 0.5 g of REM-Cl$_3 \cdot 6H_2O$ (REM= La, Ce or Nd, Sigma-Aldrich) were thoroughly mixed in an agate mortar at ambient conditions, forming a thick slurry, which was then transferred to a quartz tube furnace previously purged with 5 % $H_2/N_2$ (350 mL min$^{-1}$) for at least 30 min. The furnace temperature was increased from room temperature to 180 °C at 10 °C min$^{-1}$ and this temperature was kept for 30 min. Next, the temperature was raised at 10 °C min$^{-1}$ until 650 °C for 120 min. Finally, the furnace temperature naturally decreased to room temperature. 0.5 g of the resulting powder were washed in 500 mL of $N_2$-saturated 0.5 M $H_2SO_4$ for 4 h under magnetic stirring to remove the reaction sub-products and to induce the partial de-alloy process.[1] Finally, the catalyst was filtered under vacuum, thoroughly washed with Milli-Q water, and dried under vacuum at 80 °C overnight.

*Inductively Coupled Plasma Mass Spectrometry (ICP-MS)*.

The metal content was determined using an Agilent 7800 ICP-MS equipped with a Micromist/Scott nebulizer was used. The sample mineralization was carried out in an Anton-Paar Multiwave Pro with 600 W for 40 min.

*X-Ray diffraction (XRD)*.

The XRD patterns were recorded in a Panalytical X'Pert Pro diffractometer, equipped with a Cu K$_\alpha$ radiation source (λ=1.541 Å), using a scan rate of 0.5 ° min$^{-1}$, in the range 10 °≤ 2θ ≤ 90 °.

*Transmission Electron Microscopy (TEM)*.

Samples for TEM were prepared by suspending a small portion of the electrocatalysts in isopropanol for 30 min. An aliquot was deposited on a lacey-carbon film supported by on a copper grid and dried at room temperature. A JEOL-2200FS microscope operated at 200 kV (Schottky-FEG emitter) and fitted with an in-column omega-filter and a GATAN Ultrascan CCD 2048x2048 px² camera was used to obtain high resolution TEM (HRTEM) micrographs (0.23 nm point resolution). High-angle annular dark field STEM (HAADF-STEM) micrographs were obtained with a probe size of ranging from 0.2 nm to 1 nm (convergence semi-angle of 8 mrad and collection semi-angle greater than 80 mrad). Elemental profiles were obtained from spatially resolved electron energy loss spectroscopy (EELS) with an energy resolution of 0.9 eV as measured at the full width at half maximum (FWHM) of the zero-loss peak and a typical sampling of 0.21 nm/px (probe size of 1 nm, collection semi-angle of 8 mrad, energy dispersion of 0.086 eV/px). To prevent degradation of the samples during the electron beam irradiation, a dwell time of 100 ms (or less) was used.

Chemical maps on the $Pt_xLa/C$ nanocatalyst were recorded with a GATAN Oneview-IS 4096x4096px² CMOS camera providing faster acquisition rate (shorter dwell and readout times) than the Ultrascan camera.

*Operando X-Ray Absorption Spectroscopy (XAS)*.

X-ray absorption spectra were acquired in transmission mode at room temperature at the SAMBA beamline, Synchrotron SOLEIL, France. The beamline is equipped with a sagittally focusing Si 220 monochromator and two Pd-coated mirrors that were used to remove X-ray harmonics. The working electrode was prepared by ultrasound-dispersing 10 mg of the electrocatalyst powder in 2.98 mL of Milli-Q water, 2 mL of isopropanol and 20 µL of 5 %wt. Nafion. Then, 285 µL of the resulting suspension were carefully deposited onto *ca.* 0.785 cm² circular area of a 100 µm-thick graphite foil (Goodfellow cat. C000200/2), obtaining a Pt loading of *ca.* 200 µg cm$^{-2}$geo (the Pt *%wt.* is previously determined by ICP-MS). The working electrode was assembled in an electrochemical cell (PECC-2, Zahner), using an Hg/HgO reference electrode and a Pt wire as counter electrode. The electrochemical cell was filled with 0.1 M KOH (99.98%, semiconductor grade, Sigma-Aldrich). *Operando* XAS measurements were performed at the Pt $L_3$ edge (11564 eV) in fast acquisition mode (approx. 5 minutes for each spectrum). Five spectra were recorded at 0.1 $V_{RHE}$ to improve the signal-to-noise ratio, and the merged spectrum is reported and used for analysis.

XAS spectra were processed and analyzed using the Demeter software package (https://doi.org/10.1107/S0909049505012719). The $\chi(R)$ were modeled using single scattering paths calculated by FEFF6 with the corresponding crystalline structures of Pt5La, Pt5Ce, Pt5Nd and Pt. The amplitude reduction factor ($S_0^2$) was calculated from the fitting of the Pt foil, and it was set at 0.8 for the fitting of the materials under study. The FT-EXAFS fitting parameters, namely, the coordination number (N), Debye-Waller factor ($\sigma^2$), the energy ($\Delta E_0$) and distance ($\Delta R$) shifts, distance to neighboring atom (R), and R-factors were calculated. The used k-range and R-range in the FT-EXAFS fitting are, respectively, 3–12.6 Å$^{-1}$ and 1.7–4 Å. Besides, the relative strain $\varepsilon$ (Pt/C benchmark under same conditions) is shown. The reported values are in good agreement with previous contributions on Pt-based nanocatalysts.[2]

*Rotating-disk electrode measurements (RDE)*: The catalyst ink was prepared by dispersing *ca.* 3.6 mg of the electrocatalyst powder in 3.990 mL of Milli-Q water, 1 mL of isopropanol and 10 µL of Nafion® 5 % v/v. Then, 10 µL of the resulting suspension were deposited onto a mirror-finished glassy carbon electrode (0.196 cm²) and dried at ambient conditions by rotating the electrode at 450 rpm, obtaining a Pt loading ($L_{Pt}$) of *ca.* 10 µg$_{Pt}$ cm$^{-2}$geo (the Pt *% wt.* is previously determined by ICP-MS). A three-electrode PTFE electrochemical cell was used to avoid the detrimental effect of glass corrosion in contact with alkaline solutions,[3] where a single-junction Hg/HgO and a standard graphite rod served as reference and counter electrode, respectively. Prior to any measurement, the reference electrode was calibrated

relative to the reversible hydrogen electrode (RHE). All the reported potentials in this work are referred to the RHE. Cyclic voltammetry (CV) was carried out from 0.05 to 1.0 $V_{RHE}$ in $N_2$-saturated 0.1 M KOH (99.98%, semiconductor grade, Sigma-Aldrich). The electrochemically active surface area (ECSA) was calculated from the CO-stripping.[4] The HER/HOR polarization curves were recorded by linear sweep voltammetry, from -0.1 to 0.7 $V_{RHE}$ at 10 mV $s^{-1}$, in fresh $H_2$-saturated 0.1 M KOH. The ohmic drop was determined by electrochemical impedance spectroscopy (EIS) and compensated (85%) before running the experiment. For comparative purposes, 50 % *wt.* Pt/C from Johnson-Matthey was used as reference.

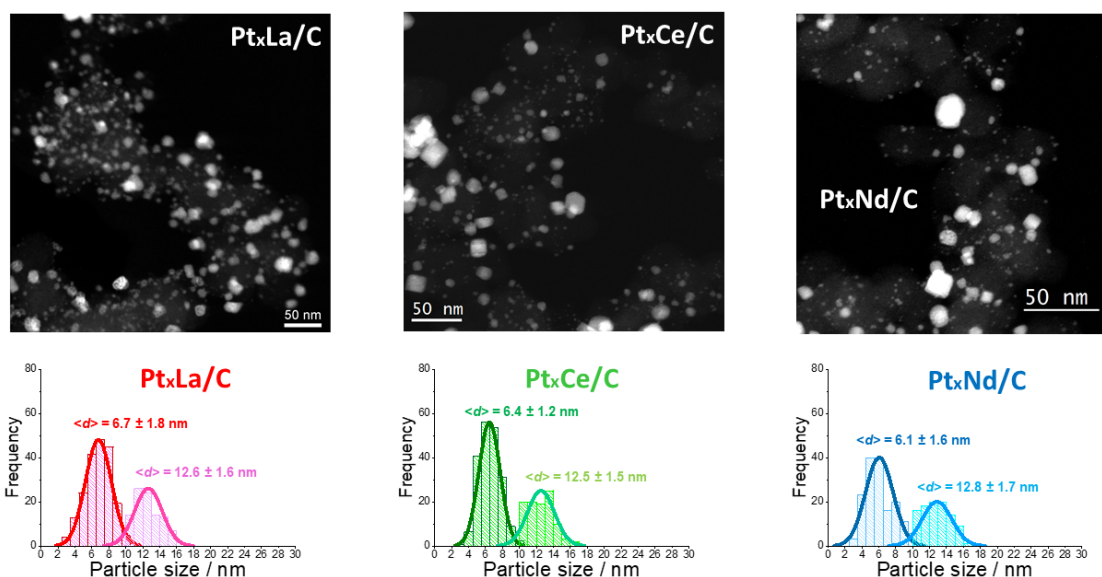## S2. Particle size distribution and *ex situ* characterization



**Figure S1**. Representative STEM micrographs of $Pt_xLa/C$, $Pt_xCe/C$ and $Pt_xNd/C$ electrocatalysts with their respective particle size histograms.

The lattice constants of the hexagonal $Pt_5RE$ crystalline structure were estimated from the XRD patterns and are shown in **Table S1**. The lattice parameter *a* and *b* of the nanoalloys series are smaller, following the lanthanide contraction, see **Scheme S1**. The nearest neighbor Pt-Pt distance in these hexagonal structures is[4]:

$$d_{Pt-Pt} = \frac{a}{2}$$

Therefore, the *ex situ* compressive strain can be expressed by:

$$\%\varepsilon_{ex\,situ} = \frac{[d_{Pt-Pt}]_{alloy} - [d_{Pt-Pt}]_{Pt}}{[d_{Pt-Pt}]_{Pt}} x100$$

where $\%\varepsilon_{ex\,situ}$ is the *ex situ* induce compressive strain; $[d_{Pt-Pt}]_{alloy}$ is the nearest neighbor Pt-Pt distance in the $Pt_5RE$ alloy; and $[d_{Pt-Pt}]_{Pt}$ is the nearest neighbor Pt-Pt distance of pure Pt nanoparticles:

$$[d_{Pt-Pt}]_{Pt} = \frac{a}{\sqrt{2}} = \frac{3.90\,Å}{\sqrt{2}} = 2.75\,Å$$

The estimated *ex situ* compressive strain of the $Pt_xRE/C$ series is shown in **Table S1**.
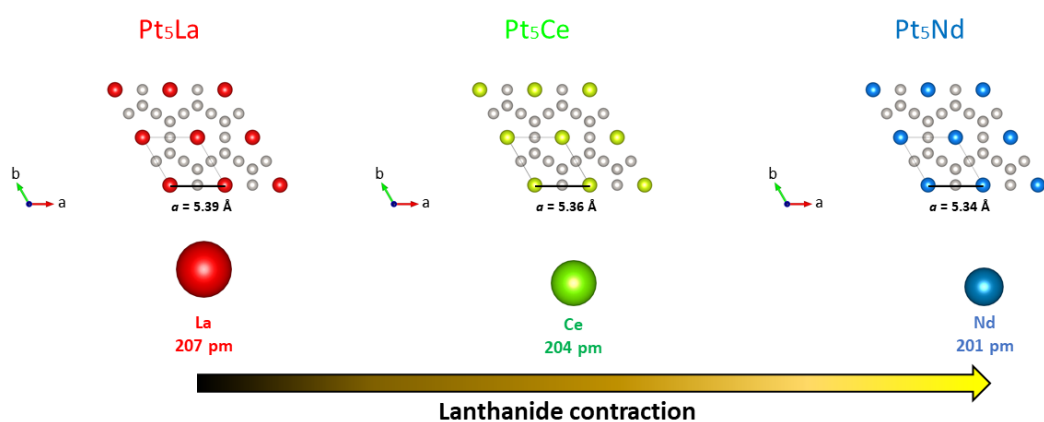


**Scheme S1**. Lattice parameter of $Pt_5La$, $Pt_5Ce$ and $Pt_5Nd$ alloys.

**Table S1**. *Ex situ* characterization and chemical composition determined by ICP-MS of $Pt_xLa/C$, $Pt_xCe/C$ and $Pt_xNd/C$.

| Sample | Crystalline structure | Lattice constants (Å) | %ε* *ex situ* | %wt. | Pt:RE (mol) | Average particle size (nm) |
|---|---|---|---|---|---|---|
| $Pt_xLa/C$ | $Pt_5La$ Hexagonal P6/mmm | a = 5.39 b = 5.39 c = 4.38 | -2.00 | Pt: 28.7 La: 3.4 | 6.0 : 1 | 6.7 ±1.8 and 12.6 ±1.6 |
| $Pt_xCe/C$ | $Pt_5Ce$ Hexagonal P6/mmm | a = 5.36 b = 5.36 c = 4.37 | -2.54 | Pt: 26.78 Ce: 3.09 | 6.3 : 1 | 6.4 ±1.2 and 12.5 ±1.5 |
| $Pt_xNd/C$ | $Pt_5Nd$ Hexagonal P6/mmm | a = 5.34 b = 5.34 c = 4.39 | -2.90 | Pt: 27.04 Nd: 3.29 | 6.1 : 1 | 6.1 ±1.6 and 12.8 ±1.7 |

* Relative to $d_{Pt-Pt}$ = 2.75 Å.

## S3. Complementary cyclic voltammograms analysis
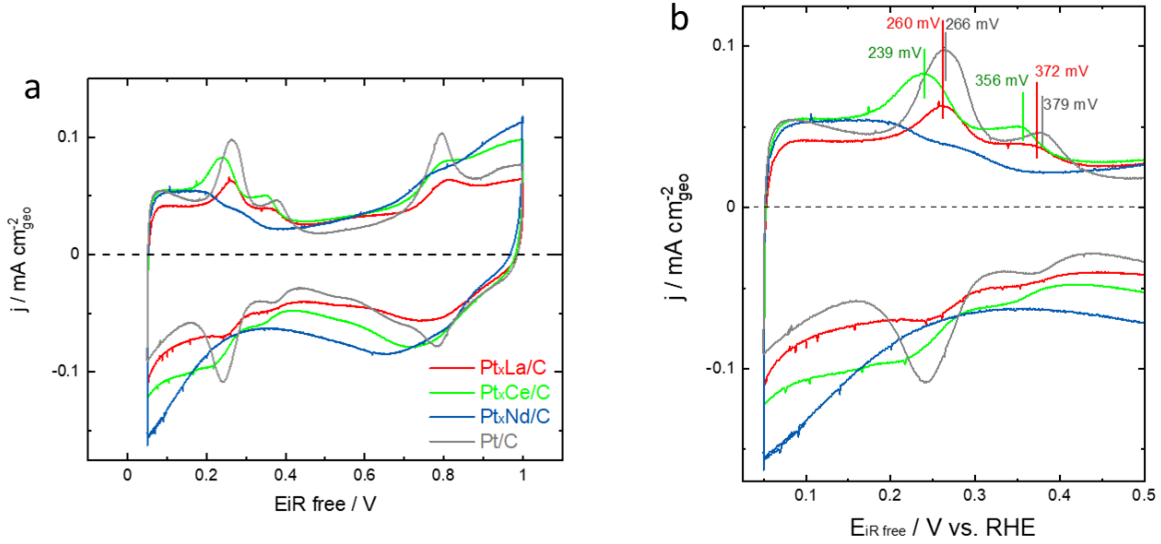


**Figure S2**. (a) Overlapped cyclic voltammograms (0.05 to 1.0 $V_{RHE}$), and (b) overlapped $H_{upd}$ region (0.05 to 0.5 $V_{RHE}$) of $Pt_xLa/C$, $Pt_xCe/C$ and $Pt_xNd/C$. Measurements were carried out in fresh $N_2$-saturated 0.1 M KOH at 26 ±1 °C. Pt/C is used as reference.


## S4. Kinetic parameters extraction

### a) ECSA determination

The electrochemically active surface area (ECSA) was calculated from the CO-stripping method. After the surface activation, the electrode potential was held at 0.1 V and CO was bubbling for 5 min. After that, the gas was switch back to $N_2$ for 20 min to remove the residual CO in the solution. Then, three potential cycles were performed between 0.05-1.0 V. The second cycle of the experiment was used as background and was subtracted from the first cycle. The CO oxidation charge was calculated by the integration of the background-corrected curve and its correction for the scan rate[6]:

$$Q = \frac{1}{v}\int i \, dE$$

The platinum surface ($S_{Pt}$) was calculated assuming a theoretical value of $Q_0 = 420$ $\mu C$ $cm_{Pt}^{-2}$ for the electro-oxidation of an adsorbed CO monolayer:

$$S_{Pt} = \frac{Q}{Q_0}$$

The ECSA was derived from the normalization of $S_{Pt}$ with respect to the Pt loading ($L_{Pt}$):

$$ECSA = \frac{S_{Pt}}{L_{Pt} \cdot A_{geo}}$$

Where $L_{Pt} = 10 \ \mu g_{Pt} \ cm_{geo}^{-2}$; $A_{geo} = 0.196 \ cm_{geo}^2$.

**b) Kinetic current**

The experimental data was analyzed following the suggestions from Prats *et al*.[7] Firstly, the HOR limiting current density, $j_{limHOR}$, was estimated from the iR-corrected polarization curves at different electrode speed rotation, see **Figure S3**, using the Levich equation.
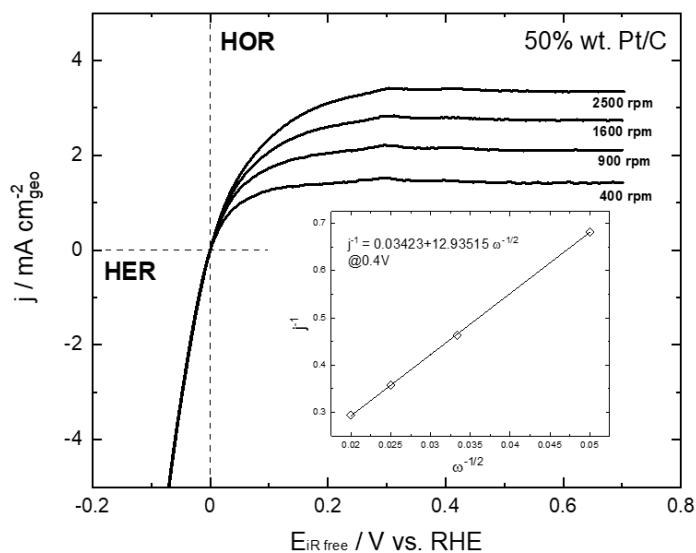


**Figure S3**. iR-corrected polarization curves at different speed rotation of Pt/C. The insert shows the relationship $j^{-1}(w^{-1/2})$ at 0.4 V.

In all cases, for the kinetic analysis, the polarization curve recorded at 1600 rpm was used. Then, the purely diffusion current density, $j_d$, was determined using the concentration overpotential curve derived from the Nernstian equilibrium (assuming infinitely fast reaction kinetics):

$$j_d = \frac{1 - e^{-\frac{nF}{RT}\eta}}{\frac{1}{j_{limHOR}} - \frac{e^{-\frac{nF}{RT}\eta}}{j_{limHER}}}$$

where n is the electron number for the HER/HOR (n=2 e⁻), F is the Faraday constant, R the universal gas constant, and T the temperature. Recently, the presence of mass transport limitations during the HER on Pt surfaces has been suggested.[4] In the case of the HER limiting current density, $j_{limHER}$, we assumed a value of -1700 mA cm⁻².[7] Then, the HER/HOR kinetic current, $j_k$, was extracted from the Koutecky-Levich equation:

$$j_k = \frac{j_d \cdot j_T}{j_d - j_T}$$

## c) Transfer coefficients

Due to coverage effects, the individual values of the anodic and cathodic transfer coefficients ($\alpha_a$ and $\alpha_c$, respectively), as well as their sum, can range from 0 to 2 for both HER and HOR.[7] Therefore, we have calculated individually each transfer coefficient as following:

$$\alpha_a = \frac{RT}{F} \frac{d}{dE} [\ln j_{k\,HOR}]$$

$$\alpha_c = \frac{RT}{F} \frac{d}{dE} [\ln |j_{k\,HER}|]$$

## d) Exchange current density and charge transfer resistance

The calculated $j_k$ was normalized by the Pt surface. Then, from the HER/HOR polarization curves, we obtained the micro-polarization region (±5 mV from equilibrium). In this region, the Butler-Volmer equation:

$$j = j_0 \left[ e^{(\alpha_a nF/RT)\eta} - e^{(\alpha_c nF/RT)\eta} \right]$$

can be linearized as:

$$j \approx j_0 \frac{(\alpha_a + \alpha_c)F}{RT} \eta$$

allowing the charge-transfer resistance estimation:

$$R_{ct} \approx \frac{RT}{F} j_0^{-1}$$

where $F = 96485.33$ C mol$^{-1}$; $T = 299.15$ K and $R = 8.3144$ J mol$^{-1}$ K$^{-1}$. Therefore, the slope of the linear fit of micro-polarization region is equivalent to the reciprocal of charge-transfer resistance.

**e) Turnover frequency**

The turnover frequency, defined as the number of $H_2$ evolved (for the HER) or consumed (for the HOR) per active site per unit time, was calculated as follows[4]:

$$TOF = \frac{i_k}{Q}$$

where $i_k$ is the kinetic current and $Q$ is the CO oxidation charge.

**f) Mass activity**

The calculated $j_k$ was normalized by the electrode Pt loading:

$$I_m = \frac{j_k}{L_{Pt}}$$
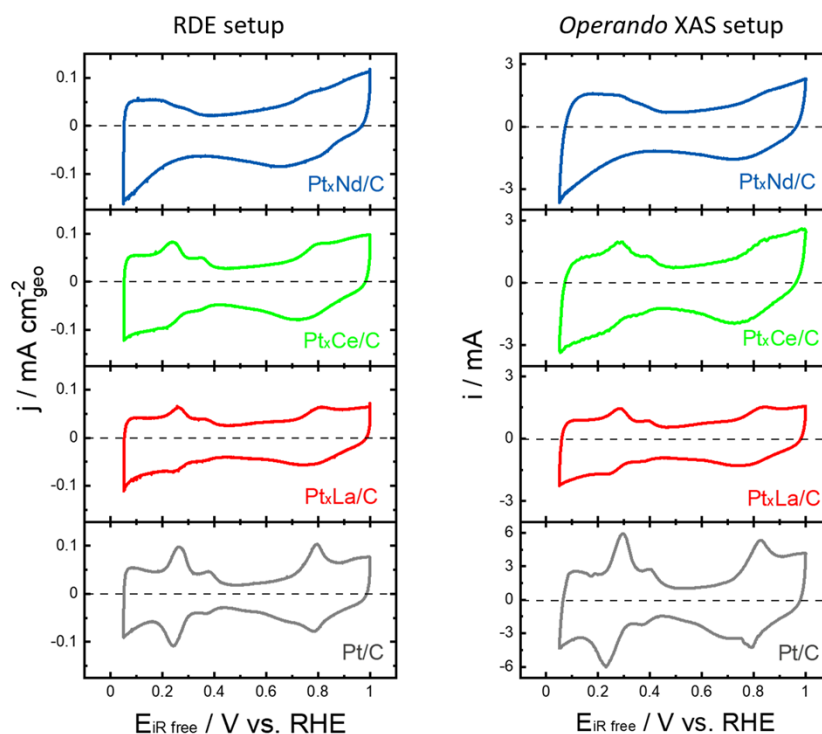
## S5. Cyclic voltammograms using different setups



**Figure S4**. Acquired cyclic voltammograms (0.05 to 1.0 $V_{RHE}$) using the RDE or the operando XAS electrochemical cell of $Pt_xLa/C$, $Pt_xCe/C$ and $Pt_xNd/C$. Measurements were carried out in fresh $N_2$-saturated 0.1 M KOH. Pt/C is used as reference.


## S6. Elemental mapping

Chemical maps of Pt and RE were obtained from STEM-EELS spectrum images following the data processing previously described.[8] The new instrumental setup allowing for a better statistics was employed for the $Pt_xLa$ case. Spectra (displayed in the second derivative mode) together with the Pt(red)/La(green)/C(blue) color maps are displayed in Figure S5. The spectrum in red extracted from the top part of the nanoparticle exhibit a lack of La compared to the green one obtained at the center of the particle. The blue spectrum extracted away from the particle shows the carbon support contribution and provides a good estimate of the background and the signal to noise ratio levels. The color map obviously reveals a red "ring" around the particle demonstrating the Pt enrichment of the shell of the particle.
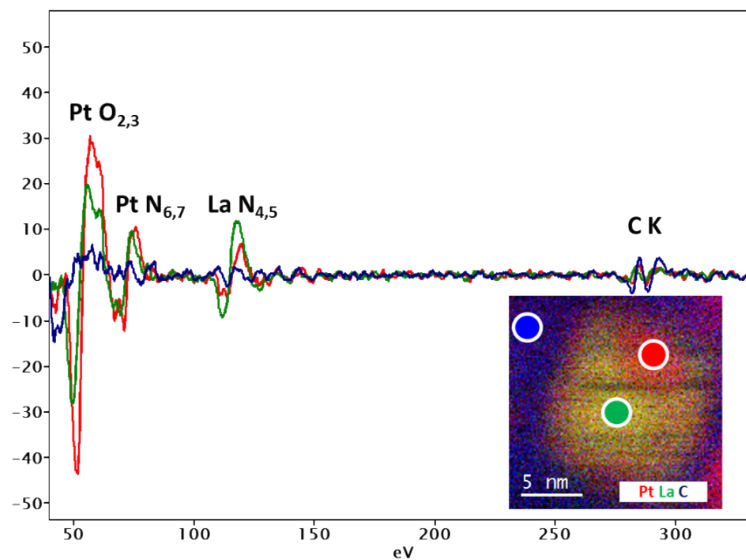
**Figure S5**. Representative EELS spectra (displayed in 2$^{nd}$ derivative mode) extracted at different locations of the spectrum-image used to produce the RVB map shown in insert.
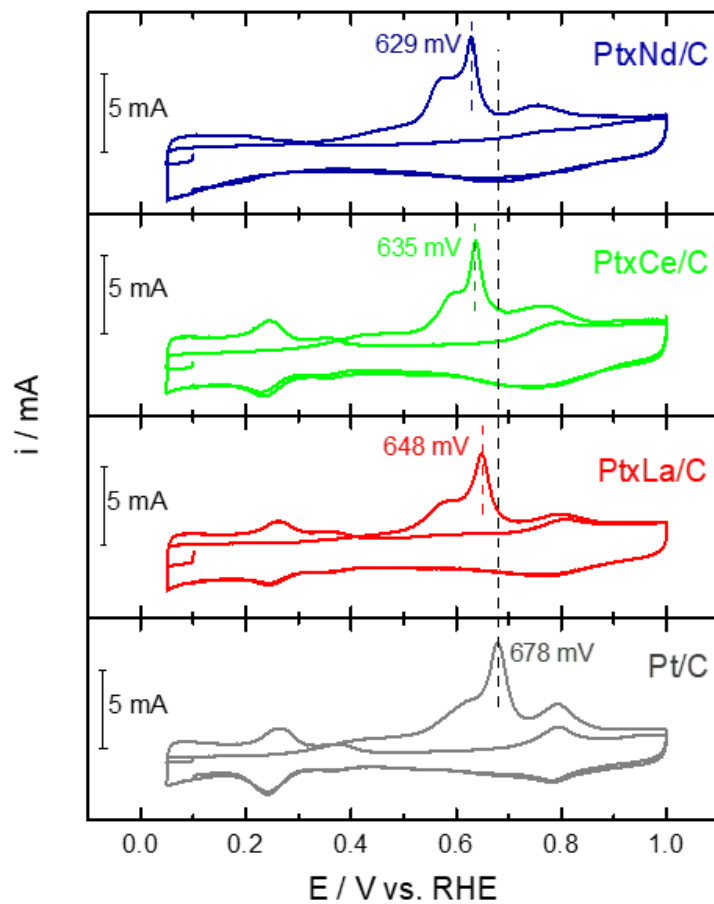
## S7. Supplementary electrochemical measurements



**Figure S6**. CO-stripping voltammograms of $Pt_xLa/C$, $Pt_xCe/C$ and $Pt_xNd/C$. Measurements were carried out in fresh $N_2$-saturated 0.1 M KOH. Pt/C is used as reference.
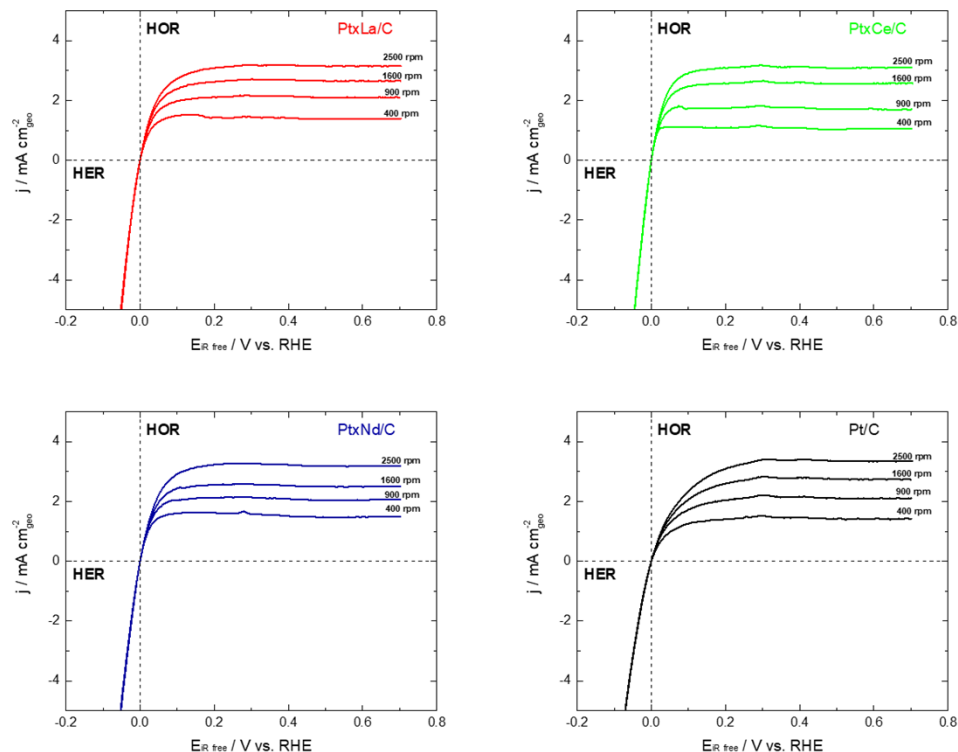
**Figure S7**. iR-corrected HER/HOR polarization curves at different speed rotation of $Pt_xLa/C$, $Pt_xCe/C$ and $Pt_xNd/C$. Measurements were carried out in fresh $H_2$-saturated 0.1 M KOH. Pt/C is used as reference.

**REFERENCES**

1.      Campos-Roldan, C. A.; Pailloux, F.; Blanchard, P. Y.; Jones, D. J.; Roziere, J.; Cavaliere, S., Enhancing the activity and stability of carbon-supported platinum-gadolinium nanoalloys towards the oxygen reduction reaction. *Nanoscale Adv* **2021,** *4* (1), 26-29.

2.      Timoshenko, J.; Roldan Cuenya, B., In Situ/Operando Electrocatalyst Characterization by X-ray Absorption Spectroscopy. *Chem Rev* **2021,** *121* (2), 882-961.

3.      Campos-Roldán, C. A.; González-Huerta, R. G.; Alonso-Vante, N., Experimental Protocol for HOR and ORR in Alkaline Electrochemical Measurements. *Journal of The Electrochemical Society* **2018,** *165* (15), J3001-J3007.

4.      Hansen, J., Prats, H., Toudahl, K., Secher, M., Chan, K., Kibsgaard, J., Chorkendorff, I., Is There Anything Better than Pt for HER? *ACS Energy Lett.* **2021,** *6*, 1175−1180.

5.      Escudero-Escribano, M.; Malacrida, P.; Hansen, M.; Vej-Hansen, U.; Velázquez-Palenzuela, A.; Tripkovic, V.; Schiøtz, J.; Rossmeisl, J.; Stephens, I.; Chorkendorff, I., Tuning the activity of Pt alloy electrocatalysts by means of the lanthanide contraction. *Science* **2016,** *352* (6281), 73-76.

6.      Mayrhofer, K. J. J.; Strmcnik, D.; Blizanac, B. B.; Stamenkovic, V.; Arenz, M.; Markovic, N. M., Measurement of oxygen reduction activities via the rotating disc electrode method: From Pt model surfaces to carbon-supported high surface area catalysts. *Electrochim Acta* **2008,** *53* (7), 3181-3188.

7.    Prats, H.; Chan, K., The determination of the HER/HOR reaction mechanism from experimental kinetic data. *Phys. Chem. Chem. Phys.* **2021,** *23*, 27150.

8.    Campos-Roldán, C. A.; Chattot, R.; Filhol, J.-S.; Guesmi, H.; Pailloux, F.; Bacabe, R.; Blanchard, P.-Y.; Zitolo, A.; Drnec, J.; Jones, D. J.; Cavaliere, S., Structure Dynamics of Carbon-Supported Platinum-Neodymium Nanoalloys during the Oxygen Reduction Reaction. *ACS Catalysis* **2023,** *13* (11), 7417-7427.